Oral Oncology 98 (2019) 118–124

Contents lists available at ScienceDirect

Oral Oncology

journal homepage: www.elsevier.com/locate/oraloncology

Leading edge or tumor core: Intratumor cancer stem cell niches in oral cavity squamous cell carcinoma and their association with stem cell function

Farshad N. Chowdhury[a], Julie Reisinger[b], Karina E. Gomez[b], Tugs-Saikhan Chimed[b], Carissa M. Thomas[c], Phuong N. Le[b], Bettina Miller[b], John J. Morton[b], Cera M. Nieto[b], Hilary L. Somerset[d], Xiao-Jing Wang[d], Stephen B. Keysar[b,*], Antonio Jimeno[a,b,*]

[a] Department of Otolaryngology, University of Colorado Denver School of Medicine (UCDSOM), Aurora, CO 80045, USA
[b] Division of Medical Oncology, Department of Medicine, UCDSOM, Aurora, CO 80045, USA
[c] Department of Otolaryngology – Head and Neck Surgery, University of Toronto, University Health Network/Princess Margaret Cancer Centre, Toronto, ON M4Y 2X5, Canada
[d] Department of Pathology, UCDSOM, Aurora, CO 80045, USA

ARTICLE INFO

Keywords:
Cancer stem cells
Stem cell niche
Head and neck neoplasms
Oral cancer
Surgical margins
Local neoplasm recurrence
Tumor microenvironment
Neoplasm invasion

ABSTRACT

Objectives: To describe differences in cancer stem cell (CSC) presence and behavior associated with their intratumor compartment of origin using a patient-derived xenograft (PDX) model of oral cavity squamous cell carcinoma (OCSCC).

Materials and methods: Four HPV-negative OCSCC PDX cases were selected (CUHN004, CUHN013, CUHN096, CUHN111) and the percentage of CSCs ($ALDH^+CD44^{high}$) was measured in the tumor Leading Edge (LE) and Core compartments of each PDX tumor case via fluorescence activated cell sorting (FACS). The fraction of cells in the proliferative phase was measured by Ki-67 labelling index of paraffin embedded tissue. The proliferation and invasion of LE versus Core CSCs were compared using sphere and Matrigel invasion assays, respectively.

Results: Both CUHN111 and CUHN004 demonstrate CSC enrichment in their LE compartments while CUHN013 and CUHN096 show no intratumor difference. Cases with LE CSC enrichment demonstrate greater Ki-67 labelling at the LE. CSC proliferative potential, assessed by sphere formation, reveals greater sphere formation in CUHN111 LE CSCs, but no difference between CUHN013 LE and Core CSCs. CUHN111 CSCs do not demonstrate an intratumor difference in invasiveness while CUHN013 LE CSCs are more invasive than Core CSCs.

Conclusion: A discrete intratumor CSC niche is present in a subset of OCSCC PDX tumors. The CSC functional phenotype with regard to proliferation and invasion is associated with the intratumor compartment of origin of the CSC: LE or Core. These individual functional characteristics appear to be modulated independently of one another and independently of the presence of an intratumor CSC niche.

Introduction

The treatment of head and neck squamous cell carcinoma (HNSCC) remains a clinical challenge given its rising overall incidence and stagnant five-year survival rate over the last decade [1–3]. Adequate surgical resection is defined by negative histologic margins, however, local recurrence occurs in up to 30% of cases in which surgical margins were negative at the time of resection [4,5]. This reality has driven an interest in molecular assessments of margin adequacy and has highlighted the importance of decoding tumor behavior at the surgical margin [6,7].

The cancer stem cell (CSC) has been proposed as one possible driver of both local recurrence and regional spread in HNSCC given the ability of a single CSC to asymmetrically divide and repopulate the tumor of origin while also resisting chemotherapy, radiotherapy, and immune surveillance [8–10]. CSCs are typically identified by a combination of cell surface protein expression and intracellular enzymatic activity, with HNSCC CSCs commonly defined by the co-expression of high levels of cell surface protein CD44 and high aldehyde dehydrogenase (ALDH) activity [11,12]. Notably, these $ALDH^+CD44^{high}$ cells also demonstrate upregulation of genes that are both associated with stemness and are putative prognostic markers of the molecular margin [13–16].

Prior studies have investigated the prognostic implications of the

* Corresponding authors at: Division of Medical Oncology, Department of Medicine, UCDSOM, Aurora, CO 80045, USA (A. Jimeno).
E-mail addresses: stephen.keysar@ucdenver.edu (S.B. Keysar), antonio.jimeno@ucdenver.edu (A. Jimeno).

https://doi.org/10.1016/j.oraloncology.2019.09.011
Received 24 May 2019; Received in revised form 2 September 2019; Accepted 10 September 2019
Available online 03 October 2019
1368-8375/

presence of these markers in the margin and margin-adjacent tissues via immunohistochemistry (IHC) with often contradictory results [17–23]. Here, we seek to further define the behavior of CSCs at the tumor leading edge (LE) by utilizing a patient-derived xenograft (PDX) model of HNSCC to identify the CSC niche and associated CSC functional phenotypes.

Methods

PDX case generation

The protocol for studies involving human subjects was approved by the Colorado Multiple Institutional Review Board (COMIRB #08-0552), and informed written consent was obtained from all patients whose tissues were used for this study. The University of Colorado Institutional Animal Care and Use Committee approved all experiments involving mice.

PDX case selection

Tissue was selected from existing PDX cases. PDX generation and characterization was previously reported [24]. Available PDX cases were narrowed to those whose originating patient case was an HPV-negative oral cavity squamous cell carcinoma (OCSCC) primary. Cases with available PDX tissue were selected: CUHN004, CUHN013, CUHN096, CUHN111.

PDX tumor digestion and FACS analysis

PDX tumors were individually sectioned using a #10 scalpel and surgical loupe magnification to produce a 2–3 mm leading edge (LE) rim of tissue and its associated tumor core of tissue. In subsequent steps, tissue was not comingled. PDX tumor tissue was finely minced with a scalpel and dissociated in DMEM containing 1 mg/ml collagenase IV (Worthington, Lakewood, NJ) at 37 °C for 1 h. Cells were filtered (40 μm) and red blood cells were lysed in Ammonimum-Chloride-Potassium (ACK) lysing buffer (Life Technologies, Carlsbad, CA). Staining with Aldefluor (Stem Cell Technologies, Vancouver, Canada) was performed following the manufacturer's instructions. Briefly, cells were suspended in Aldefluor staining buffer containing Aldefluor reagent (5 μl/ml) and incubated at 37 °C for 30 min. DEAB (N,N-diethylaminobenzaldehyde) was used as a negative control for setting gates. Following incubation with Aldefluor, cells were stained with the following antibodies: 1:100 anti-mouse H-2Kd (BioLegend, San Diego, CA), 1:10 anti-human CD44 (BD Biosciences, San Jose, CA) with species specificity validated by the manufacturer. Cell sorting was performed using a MoFlo XDP (Beckman Coulter, Fort Collins, CO) and flow cytometric analysis was completed on a Gallios 561 (Beckman Coulter). In order to select only live, human, CSCs for subsequent functional assays we gated anti-mouse $H2kd^{-}/DAPI^{-}$ to exclude mouse cells and dead cells prior to gating on our $ALDH^{+}/CD44^{high}$ cells of interest (Supplemental Fig. 1).

Supplementary data associated with this article can be found, in the online version, at https://doi.org/10.1016/j.oraloncology.2019.09.011.

Sphere assay

Tumors were harvested, sectioned into LE and Core compartments, and processed to single cell suspension for FACS as described above. $ALDH^{+}CD44^{high}$ CSCs were sorted and collected. Cells were plated at 5000 cells per well in 96-well ultra-low attachment plates in 150 μl of serum-free media (DMEM F12 [Gibco], 20 ng/mL recombinant human epithelial growth factor, 20 ng/mL recombinant human fibroblast growth factor, and 1x B27 supplement) for 12 days. Spheres were imaged, measured, and quantified using Zeiss Axio Observer Z1 inverted microscope (Zeiss, Oberkochen, Germany) (Zeiss software Rel. 4.8). 3D structures larger than 30 μm were scored as spheres. Relative Sphere Formation was calculated by normalizing the sphere formation counts of each condition to the average Core sphere formation count.

Immunohistochemistry (IHC)

Slides were de-paraffinized and re-hydrated in graded concentrations of alcohol by standard techniques before antigen retrieval in citrate buffer pH 6.0 (#S1699 Dako) at 121 °F for 10 min. Next, the slides were cooled for 20 min before washing in wash buffer (#K8007 Dako). All staining was done in a Dako Autostainer. Slides were incubated in dual endogenous enzyme block (#S2003 Dako) for 10 min, and in protein free blocking solution (#X0909 Dako) for 20 min, followed by primary antibody (1:100 #RM-9106-S Thermoscientific Ki-67) and incubated for 60 min at room temperature. Staining was developed using the following conditions: EnVision + Dual Link System HRP (#K4061 Dako) for 30 min and substrate-chromogen (DAB +) Solution (#K3468 Dako) for 5 min. Slides were counterstained with hematoxylin (#S3301 Dako) for 10 min.

Ki-67 labeling index

To calculate the Ki-67 labeling index, a PDX tumor from each of the xenograft cases of interest was stained for Ki-67 as above. Three 5x high-powered fields (HPFs) were selected from the strongest staining areas of the LE and Core areas in each case. The number of nucleated and Ki-67 positive cells was then scored automatically using a thresholding analysis in Image-J (Fiji distribution) [25] and a percentage of Ki-67 positive cells was calculated and reported in triplicate as the labelling index.

In vitro Matrigel-coated invasion assay

CUHN111 and CUHN013 PDX tumors were harvested, sectioned into Core and LE compartments, and processed to separate single cell suspensions for the LE and Core for FACS as described above. LE and Core $ALDH^{+}CD44^{high}$ CSCs were sorted and collected. Corning BioCoat Matrigel-coated 8 μm pore PET membrane 24 well inserts (Corning, Corning, NY) were brought to room temperature and hydrated in serum DMEM media for 2 h at 37 °C in a humidified tissue culture incubator, 5% CO_2 atmosphere. $2x10^5$ LE and Core CSCs were separately added to the inserts in DMEM containing 0.5% FBS while DMEM containing 10% FBS was used as a chemoattractant. Plates were incubated for 72 h before fixing with 10% formalin (15 min) and staining with 0.5% crystal violet (15 min). Invasion was quantified as the total number of invaded cells over the entirety of the membrane at 5X magnification. Relative Invasion was calculated by normalizing the absolute number of invaded cells in each condition to the average number of invaded cells in the Core condition for that given experiment.

Statistical analysis

Differences in CSC composition of PDX tumor compartments were analyzed using two-tailed ratio paired t-tests. Sphere size differences were analyzed using two-tailed unpaired t-tests, and Relative Sphere Formation was analyzed using two-tailed ratio paired t-tests. Ki-67 labeling indices and normalized relative invasion values were compared using two-tailed unpaired t-tests. All alpha was set at 0.05. Column statistics, computations, and analyses were performed in Graphpad Prism v8.0.0.

1A

Case	Gender	Age at Diagnosis	Primary Site	TNM Staging	HPV Status	Primary or Recurrence	Tissue Differentiation
CUHN004	Male	55	Floor of Mouth	cT3N1M0	Negative	Local Recurrence	Moderate
CUHN013	Female	73	Floor of Mouth	cT3N2cM0	Negative	Primary	Moderate
CUHN096	Male	69	Oral Tongue	cT2N2bM0	Negative	Local Recurrence	Poor
CUHN111	Female	61	Floor of Mouth	pT2N2cM0	Negative	Primary	Poor

1B

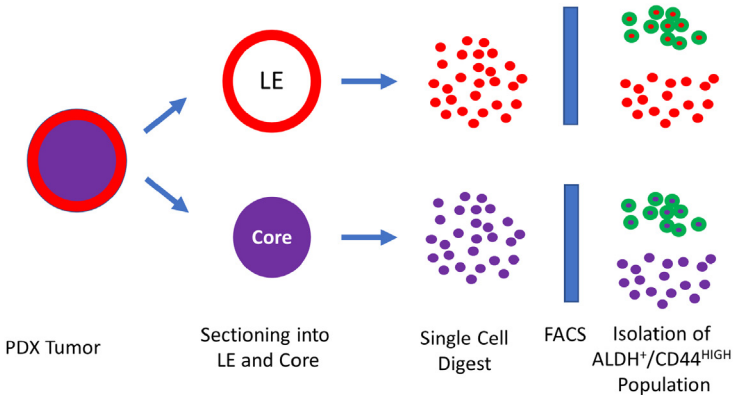

Fig. 1. CSC isolation schematic and overview of selected cases. (1A) Profiles of included PDX cases. (1B) Schematic of PDX tumor processing wherein whole PDX tumors are grossly sectioned into leading edge and core components and then digested to a single-cell suspension before incubating with CD44 and Aldefluour assay prior to FACS.

Results

PDX case demographics

Fig. 1A describes four patient-derived xenografts (PDXs) generated from HPV-negative oral cavity squamous cell cancer (OCSCC) patients. Male and female gender was represented equally, and the mean age of all patients was 64.5 years (SEM ± 4.03). The primary tumor was in the floor of mouth in three of four cases (75%), and the engrafted tissue was resected from a first primary lesion in two of the four cases (50%).

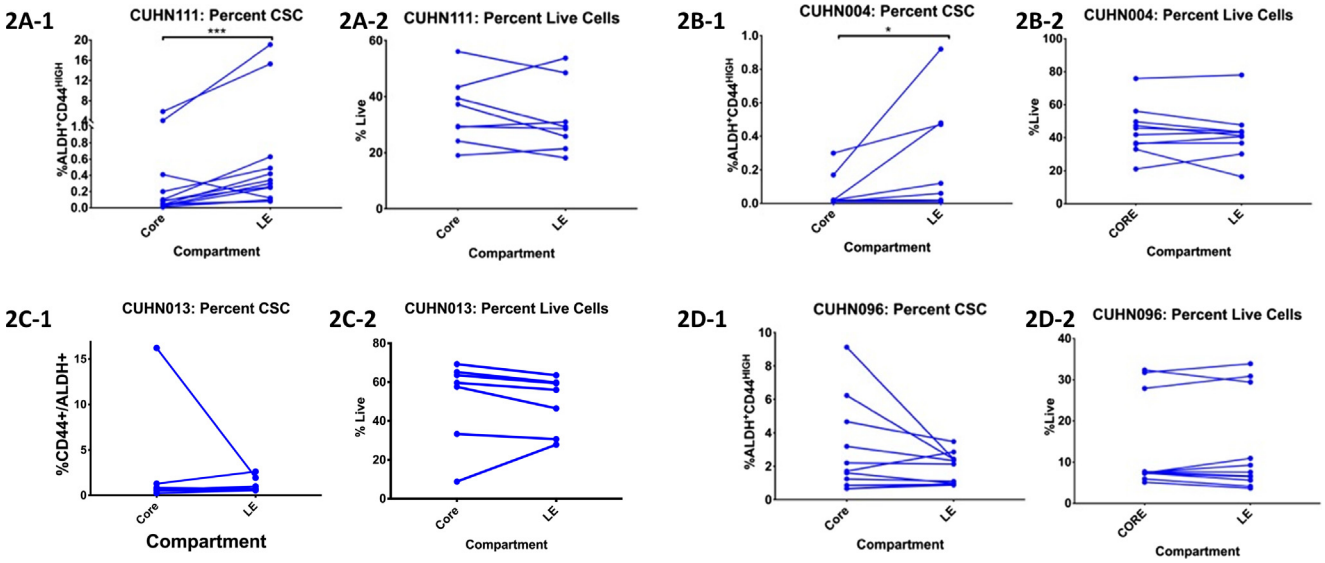

Fig. 2. ALDH$^+$/CD44^{HIGH} enrichment by tumor compartment. Each pair of connected points represents the LE and Core compartments belonging to the same individual PDX tumor. (2A-1 and 2B-1) Cases CUHN111 and CUHN004 both demonstrate ALDH$^+$CD44^{HIGH} enrichment of the LE compartment (geometric mean CUHN111 LE:Core Ratio 3.74 ± 0.124, p = 0.0006; geometric mean CUHN004 LE:Core Ratio 2.80 ± 0.457, p = 0.0129). (2C-1 and 2D-1) In contrast, CUHN013 and CUHN096 do not demonstrate a preferential localization of ALDH$^+$CD44^{HIGH} cells to a given compartment (geometric mean CUHN013 LE:Core Ratio 0.980 ± 0.165, p = 0.958; geometric mean CUHN096 LE:Core ratio 1.23 ± 0.073, p = 0.247). (2A-2–2D-2) There is no intratumor difference in the percent live cells at the time of sorting (geometric mean CUHN111 LE:Core Ratio 1.10 ± 0.033, p = 0.265; geometric mean CUHN004 LE:Core Ratio 1.07 ± 0.037, p = 0.467; geometric mean CUHN013 LE:Core Ratio 1.08, p = 0.677; geometric mean CUHN096 LE:Core Ratio 0.951 ± 0.0304, p = 0.484).

All cases were staged T2 or greater, all cases demonstrated nodal disease (either clinical or pathological based on neck dissection specimens), and none demonstrated distant metastasis at the time of resection.

HNSCC CSCs demonstrate different intratumor niches

FACS was used to determine the distribution of $ALDH^+CD44^{high}$ double-positive tumor cells by comparing the cellular composition of the leading edge (LE, outer 2–3 mm) and Core tissue compartments of individual xenograft tumors (Fig. 1B). The percent $ALDH^+CD44^{high}$ cells out of the total live, human cell population was calculated for each compartment on a tumor-by-tumor basis (Supplemental Fig. 1). Ratio paired t-tests were utilized to compare compartment composition while accounting for baseline differences in the overall $ALDH^+CD44^{high}$ population across individual xenograft tumors of a given parent case (Fig. 2). Two cases, CUHN111 and CUHN004, demonstrated $ALDH^+CD44^{high}$ enrichment of the respective LE compartments (CUHN111 LE:Core Ratio 3.74 ± 0.12, $p < 0.001$; CUHN004 LE:Core Ratio 2.80 ± 0.46, $p = 0.013$, Fig. 2A-1 and 2B-1). Neither CUHN111 nor CUHN004 demonstrated significant differences in the percent live cells of the overall sorted population (Fig. 2A-2 and 2B-2). Conversely, neither CUHN013 nor CUHN096 demonstrate $ALDH^+CD44^{high}$ enrichment (CUHN013 LE:Core Ratio 0.94 ± 0.12, $p = 0.822$; CUHN096 LE:Core ratio 1.23 ± 0.07, $p = 0.247$, Fig. 2C-1 and 2D-1). Again, there was no intratumor difference in the percent live cells in the sorted populations in the two compartments (Fig. 2C-2 and 2D-2). These data suggest that CSCs are enriched within a tumor LE niche in a subset of OCSCC cases.

Tumor proliferation measured by Ki-67 labeling index varies by tumor compartment

Ki-67 labeling index was used to investigate differences in the proliferating fraction of the bulk tumor cells within the LE and Core compartments of PDX tumors. The degree of tumor proliferation as measured by Ki-67 labeling index is greater in the LE of CUHN111 (LE 0.587 ± 0.038, vs Core 0.236 ± 0.037, $p = 0.001$, Fig. 3A) and CUHN004 (LE 0.457 ± 0.027, vs Core 0.174 ± 0.035, $p = 0.003$, Fig. 3B). There is no difference in Ki-67 labelling index between compartments of CUHN013 (Fig. 3C) and CUHN096 (Fig. 3D). Taken with the CSC localization data (Fig. 2), those cases with CSC enrichment within a LE intratumor niche demonstrate a greater fraction of cells in the proliferative phase at the tumor LE.

Relative sphere formation of $ALDH^+CD44^{high}$ cells is associated with intratumor location

CUHN111 and CUHN013 PDX cases were selected for further analysis based on the availability of adequate PDX tissue and due to their opposing CSC localization patterns (Fig. 2). Sorted $ALDH^+CD44^{high}$ cells were seeded in a sphere formation assay to asses for functional differences in proliferation based on the intratumor location of the $ALDH^+CD44^{high}$ cells. The size of the sphere produced did not differ based on whether the $ALDH^+CD44^{high}$ cells were isolated from the LE or Core of the PDX tumor (Fig. 4A). When comparing relative sphere formation (RSF), the CUHN111 LE $ALDH^+CD44^{high}$ cells demonstrate greater sphere-forming ability than those in the Core (geometric mean LE:Core RSF 1.80 ± 0.57, $p = 0.011$, Fig. 4B). In contrast, there was no difference in the RSF of $ALDH^+CD44^{high}$ cells between the LE and Core compartments of CUHN013 (Fig. 4C). Together, these results suggest that CSCs within a LE CSC niche demonstrate greater proliferative activity than do their counterpart CSCs in the tumor core. CSCs in cases with no discrete intratumor CSC niche show no difference in proliferative activity.

Invasive potential varies by tumor compartment

Sorted $ALDH^+CD44^{high}$ cells from both the LE and Core were seeded in Matrigel coated invasion chambers to assess for differences in invasiveness. The CUHN111 LE CSCs demonstrate no greater relative invasion than those of the CUHN111 Core (Fig. 5A). In contrast, CUHN013 LE CSCs clearly demonstrate greater relative invasion than those of the CUHN013 Core (LE 8.536 ± 1.12, vs Core 1.00 ± 0.637, $p < 0.0001$, Fig. 5B). While the CUHN111 LE CSCs occupy an enriched CSC niche with an increased cellular growth fraction and greater CSC proliferation, these LE CSCs do not show greater invasiveness than those in the CUHN111 Core. Though the LE CSCs of CUHN013 neither occupy an enriched CSC niche nor display enhanced proliferative ability, these LE CSCs do demonstrate greater relative invasion than their Core counterparts.

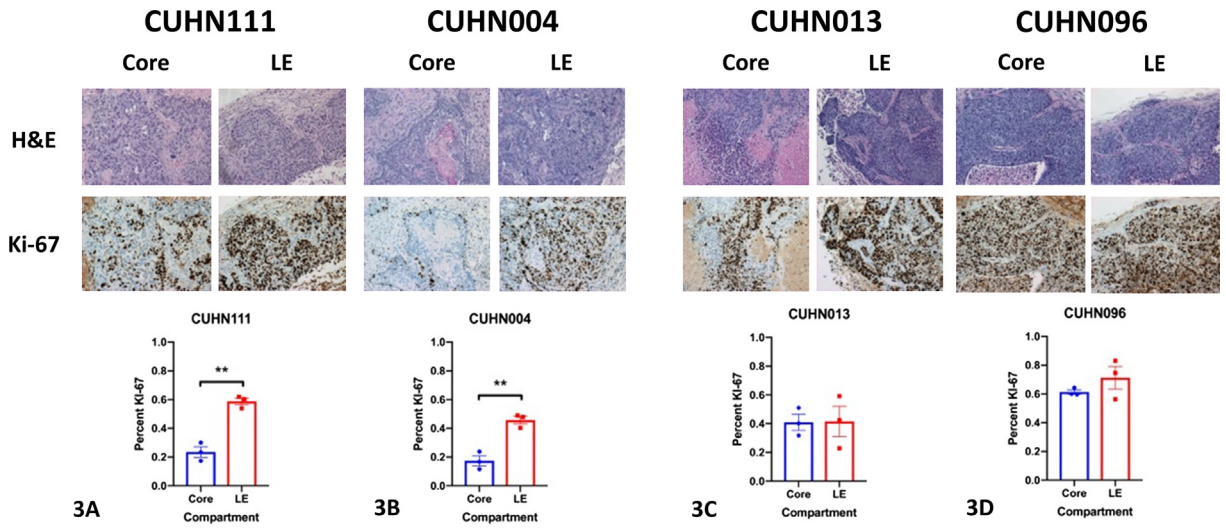

Fig. 3. KI-67 labeling index by tumor compartment. In both CUHN111 (3A) and CUHN004 (3B), the leading edge compartment demonstrates a higher KI-67 labeling index than the respective core compartment (CUHN111 LE 0.587 ± 0.038, vs Core 0.236 ± 0.037, $p = 0.001$; CUHN004 LE 0.457 ± 0.027, vs Core 0.174 ± 0.035, $p = 0.003$). In contrast, there is no difference in the KI-67 labelling index between the core and leading edge compartments of CUHN013 (LE 0.415 ± 0.105, vs Core 0.410 ± 0.056, $p = 0.967$, 3C) and CUHN096 (LE 0.713 ± 0.078, vs Core 0.613 ± 0.015, $p = 0.283$, 3D). Representative micrographs of 10x HPF for each case are shown. Three 10x HPF of the greatest staining area within each compartment were scored for analysis.

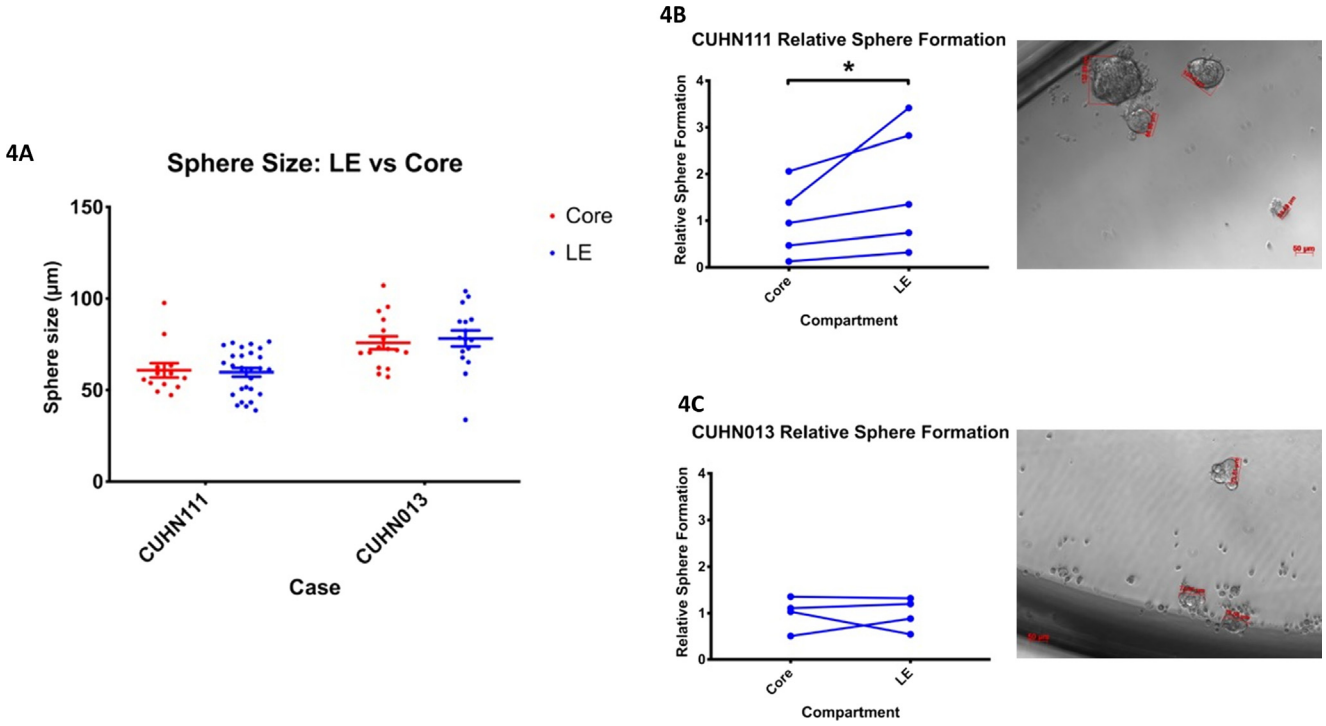

Fig. 4. CSC relative sphere formation differs by CSC compartment of origin. (4A) There is no significant intra-tumoral difference in the size of sphere generated by the LE CSCs vs Core CSCs (CUHN111 59.7μ ± 2.29 vs 60.75μ ± 3.85, p = 0.803; CUHN013 78.2μ ± 4.37 vs 75.8μ ± 3.55, p = 0.673. (4B) Each pair of connected points represents the LE and Core compartments belonging to the same individual PDX tumor. CUHN111 demonstrates greater LE compartment CSC sphering efficiency as measured by relative sphere formation (geometric mean LE:Core RSF 1.80 ± 0.57, $p = 0.011$). (4C) CUHN013 demonstrates no functional difference in CSC sphering between compartments (geometric mean LE:Core RSF 0.99 ± 0.11, $p = 0.976$).

Discussion

In solid tumors, CSCs have the ability to faithfully recapitulate the parent tumor and therefore garner attention as possible drivers for tumor recurrence [10]. Furthermore, CSCs may contribute to treatment resistance through their relative chemoresistance, radioresistance, and potential for immune evasion [9,10,26,27]. The role of CSCs in HNSCC is of particular interest given that the overall five-year survival rate has not improved from 50 to 70% over the course of the last decade [1–3] and that the rate of local recurrence is as high as 30% even in the setting of negative surgical margins [4,5]. This presents a special challenge in the treatment of the OCSCC subgroup where the primary modality of treatment is surgical resection [28]. In our view, an understanding of the distribution of CSCs in HNSCC/OCSCC may provide

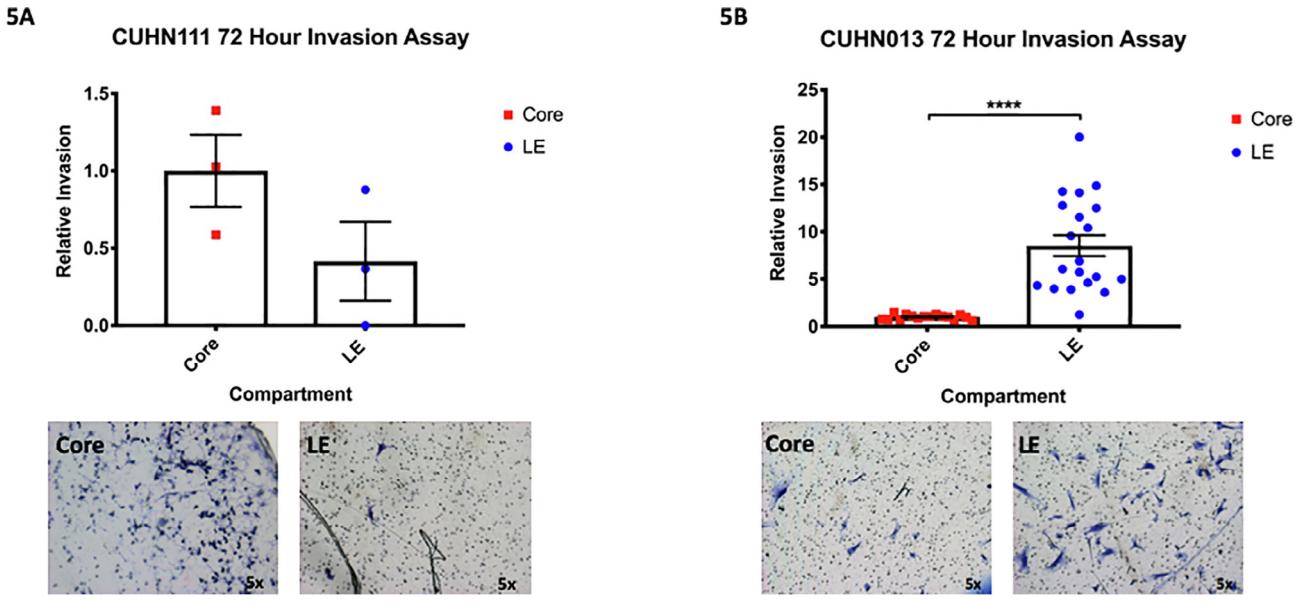

Fig. 5. CUHN013 LE CSCs have greater invasive ability than core CSCs. Each point represents an individual invasion well. (5A) In CUHN111 there is no difference in invasive behavior between CSCs isolated from the core as compared to the LE (LE 0.415 ± 0.255, n = 3, vs Core 1.00 ± 0.233, n = 3, p = 0.165). (5B) CSCs in the CUHN013 LE demonstrate greater invasion than those isolated from the tumor core as measured by relative invasion (LE 8.536 ± 1.12, n = 20, vs Core 1.00 ± 0.637, n = 16, p < 0.0001).

insight into the mechanisms of multimodal treatment failure and disease recurrence.

Normal stem cells are known to occupy niches in which a specific microenvironment supports the stem cell phenotype and homeostasis [29,30]. This observation has extended to the realm of CSCs through the concepts of the inducing or supportive CSC niches. Models for CSC/niche interaction include the cooptation of the normal stem cell niche or other existing favorable niche (e.g. the perivascular niche) and CSC induction or support via the existing micro-environment at the tumor-stroma-interface [30,31]. The influence of the LE microenvironment may serve as a selective pressure for a LE intratumor niche of CSCs [31–33]. The intratumor distribution of CSCs within solid tumors has not been well described, and its potential impact on surgical margins and tumor recurrence is not well understood.

Here we describe a discrete intratumor CSC niche as defined by regional enrichment of the $ALDH^+CD44^{high}$ cell population in our HNSCC PDX model. Prior work by our group has affirmed that $ALDH^+CD44^{high}$ cells isolated from our HNSCC PDX models demonstrate asymmetric cell division and possess increased stem-like characteristics, tumorigenicity, and treatment resistance when compared to the bulk tumor cell population [8]. Here we report that in a subset of our OCSCC cases (CUHN111 and CUHN004), the grossly sectioned 2–3 mm tumor leading edge demonstrates an enrichment of CSCs by 3.74 and 2.80 fold, respectively (Fig. 2), when compared to the corresponding tumor core, which itself is not devoid of CSCs. While the absolute CSC population is variable between OCSCC tumor cases, OCSCC CSCs demonstrate the same tumorigencity when compared cell to cell, therefore lending an intercompartment fold change comparison reasonable biological relevance [8]. This enrichment is observed in individual PDX tumors across implant generations which suggests that the observed LE CSC intratumor niche is a property inherent to the parent OCSCC case. While CUHN013 and CUHN096 also possess a measurable $ALDH^+CD44^{high}$ cell population, there is no discrete intratumor CSC niche as defined by a relative enrichment of CSCs in either the LE or Core compartments. The differences in the presence and absence of an intratumor CSC niche between CUHN111/CUHN004 and CUHN013/CUHN096 is reflective of the previously observed intratumor molecular heterogeneity in HNSCC as a whole [34–36].

The functional profiles of our OCSCC CSCs vary based on their intratumor compartment of origin. CSCs isolated from the CUHN111 LE demonstrate greater sphere formation and thereby greater proliferative ability than the identically isolated CSCs from the Core compartment of the same PDX tumor. CUHN111 and CUHN004 appear to possess a LE intratumor CSC enriched niche, and the corresponding bulk tumor cell population of this LE niche demonstrates a greater fraction of cells in the proliferative phase when compared with the tumor core cell population. While CUHN111 CSCs vary in the proliferative profile based on their intratumor compartment, they do not vary in their invasive capacity. In contrast, CUHN013 CSCs do not demonstrate intratumor variation in proliferative ability but do demonstrate a clear intratumor variation in invasive capacity. Functional specialization does not appear to require the presence of a discrete CSC niche, as the greater relative invasion demonstrated by CUHN013 LE CSCs is observed in a case where there is in fact no intratumor compartment with CSC enrichment.

Invading cells in solid cancers – including HNSCC – demonstrate epithelial to mesenchymal (EMT) and mesenchymal to epithelial (MET) transitions which may represent a mechanism for local invasion and distant metastasis, and solid tumor CSCs may undergo EMT/MET under the influence of the local tumor microenvironment (TME) [31,32]. This plasticity of CSCs based on signaling in the TME serves as a strategy for tumor growth and proliferation [34]. In prostate cancer, the TME of a coopted stem cell niche has the capacity to skew differentiated disseminated tumor cells towards a CSC phenotype through the Mer/mTOR pathway [37], and prostate CSCs may consist of both stationary and metastatic populations [38]. However, in OCSCC, the presence of a CSC niche and its impact on CSC functional phenotype has not been previously described. Our data suggest that CSCs isolated from a given OCSCC case – while defined by identical isolation criteria – do not represent a monolithic population. Instead, there are discrete OCSCC CSC functional subtypes with regard to the properties of proliferation and invasion. Furthermore, these functional subtypes are found within distinct and at times mutually exclusive intratumor regions. This level of variability in CSC function – both between OCSCC cases and within individual tumors – may be a possible explanation for extant contradictory results regarding the prognostic value of stemness related markers at the molecular margin. The presence of OCSCC CSCs with distinct functional phenotypes highlights the need for further investigation into tumor and microenvironment signaling mechanisms that modulate these CSC characteristics.

The generalizability of the conclusions of our study is constrained by a set of practical limitations, beginning with the small number of distinct OCSCC cases included in our investigation. In certain circumstances, tissue availability was limited by tumor growth dynamics, and enough tissue was not available to perform every functional assay on every OCSCC case. In particular, HNSCC heterogeneity resulting in variably limited tissue availability is notable in our assay of CSC invasive potential. Lastly, a number of our functional assays are descriptive and hypothesis-generating. Future work should focus further on the mechanisms underlying the observed differences in CSC phenotype and on the TME interactions that support the niche and these functional differences.

Conclusion

Here we identify a subset of OCSCC PDX tumors that demonstrate a discrete intratumor CSC niche. The functional profile – with regard to proliferation and invasion – of the CSCs within these PDX tumors varies based on the tumor compartment of origin: LE or Core. Notably, these individual functional characteristics are modulated independently of one another and independently of the presence of an intratumor CSC enriching niche.

Funding

This work was supported by National Institutes of Health grants R01-CA149456 (A.J.), R21-DE019712 (A.J.), R01-DE024371 (A.J.), P30-CA046934 (University of Colorado Cancer Center Support Grant, A.J.), T32-DC012280 (F.C.), NIH/NCATS Colorado CTSA TL1-TR002533 (K.G.), R01CA149456-07S1 (C.N), the Daniel and Janet Mordecai Foundation (A.J.), and the Peter and Rhonda Grant Foundation (A.J.).

Declaration of Competing Interest

The authors declare that they have no known competing financial interests or personal relationships that could have appeared to influence the work reported in this paper.

References

[1] Siegel RL, Miller KD, Jemal A. Cancer statistics, 2015. CA Cancer J Clin 2015;65:5–29. https://doi.org/10.3322/caac.21254.
[2] Siegel RL, Miller KD, Jemal A. Cancer statistics, 2016. CA Cancer J Clin 2016;66:7–30. https://doi.org/10.3322/caac.21332.
[3] Siegel RL, Miller KD, Jemal A. Cancer statistics, 2018. CA Cancer J Clin 2018;68:7–30. https://doi.org/10.3322/caac.21442.
[4] Hinni ML, Ferlito A, Brandwein-Gensler MS, Takes RP, Silver CE, Westra WH, et al. Surgical margins in head and neck cancer: a contemporary review. Head Neck 2012;35:1362–70. https://doi.org/10.1002/hed.23110.
[5] Leemans CR, Tiwari R, Nauta JJ, van der Waal I, Snow GB. Recurrence at the primary site in head and neck cancer and the significance of neck lymph node metastases as a prognostic factor. Cancer 1994;73:187–90.
[6] Wolf GT. Surgical margins in the genomic era: the Hayes Martin Lecture, 2012. Arch Otolaryngol Head Neck Surg 2012;138:1001–13. https://doi.org/10.1001/2013.

jamaoto.82.
[7] Mao L, Clark D. Molecular margin of surgical resections-where do we go from here? Cancer 2015;121:1914–6. https://doi.org/10.1002/cncr.29299.
[8] Keysar SB, Le PN, Miller B, Jackson BC, Eagles JR, Nieto C, et al. Regulation of head and neck squamous cancer stem cells by PI3K and SOX2. JNCI J Natl Cancer Inst 2017;109:djw189. https://doi.org/10.1093/jnci/djw189.
[9] Islam F, Gopalan V, Smith RA, Lam AKY. Translational potential of cancer stem cells: a review of the detection of cancer stem cells and their roles in cancer recurrence and cancer treatment. Exp Cell Res 2015;335:135–47. https://doi.org/10.1016/j.yexcr.2015.04.018.
[10] Mannelli G, Gallo O. Cancer stem cells hypothesis and stem cells in head and neck cancers. Cancer Treat Rev 2012;38:515–39. https://doi.org/10.1016/j.ctrv.2011.11.007.
[11] Keysar SB, Jimeno A. More than markers: biological significance of cancer stem cell-defining molecules. Mol Cancer Ther 2010;9:2450–7. https://doi.org/10.1158/1535-7163.MCT-10-0530.
[12] Prince ME, Sivanandan R, Kaczorowski A, Wolf GT, Kaplan MJ, Dalerba P, et al. Identification of a subpopulation of cells with cancer stem cell properties in head and neck squamous cell carcinoma. Proc Natl Acad Sci 2007;104:973–8. https://doi.org/10.1073/pnas.0610117104.
[13] van Houten VMM, Leemans CR, Kummer JA, Dijkstra J, Kuik DJ, van den Brekel MWM, et al. Molecular diagnosis of surgical margins and local recurrence in head and neck cancer patients: a prospective study. Clin Cancer Res 2004;10:3614–20. https://doi.org/10.1158/1078-0432.CCR-03-0631.
[14] Sterz CM, Kulle C, Dakic B, Makarova G, Böttcher MC, Bette M, et al. A basal-cell-like compartment in head and neck squamous cell carcinomas represents the invasive front of the tumor and is expressing MMP-9. Oral Oncol 2010;46:116–22. https://doi.org/10.1016/j.oraloncology.2009.11.011.
[15] Fraga CAde C, Oliveira MVMde, Domingos PLB, Botelho ACde C, Guimarães ALS, Teixeira-Carvalho A, et al. Infiltrating CD57 + inflammatory cells in head and neck squamous cell carcinoma. Appl Immunohistochem Mole Morphol 2012;20:285–90. https://doi.org/10.1097/PAI.0b013e318228357b.
[16] Major AG, Pitty LP, Farah CS. Cancer stem cell markers in head and neck squamous cell carcinoma. Stem Cells Int 2013;2013:1–13. https://doi.org/10.1007/s11912-010-0087-2.
[17] Lee SH, Oh S-Y, Do SI, Lee HJ, Kang HJ, Rho YS, et al. SOX2 regulates self-renewal and tumorigenicity of stem-like cells of head and neck squamous cell carcinoma. Br J Cancer 2014;111:2122–30. https://doi.org/10.1038/bjc.2014.528.
[18] Li W, Li B, Wang R, Huang D, Jin W, Yang S. SOX2 as prognostic factor in head and neck cancer: a systematic review and meta-analysis. Acta Otolaryngol 2014;134:1101–8. https://doi.org/10.3109/00016489.2014.913311.
[19] Tang X-B, Shen X-H, Li L, Zhang Y-F, Chen G-Q. SOX2 overexpression correlates with poor prognosis in laryngeal squamous cell carcinoma. Auris Nasus Larynx 2013;40:481–6. https://doi.org/10.1016/j.anl.2013.01.003.
[20] Bochen F, Adisurya H, Wemmert S, Lerner C, Greiner M, Zimmermann R, et al. Effect of 3q oncogenes SEC62 and SOX2 on lymphatic metastasis and clinical outcome of head and neck squamous cell carcinomas. Oncotarget 2017;8:4922–34. https://doi.org/10.18632/oncotarget.13986.
[21] Bayo P, Jou A, Stenzinger A, Shao C, Gross M, Jensen A, et al. Loss of SOX2 expression induces cell motility via vimentin up-regulation and is an unfavorable risk factor for survival of head and neck squamous cell carcinoma. Mol Oncol 2015;9:1704–19. https://doi.org/10.1016/j.molonc.2015.05.006.
[22] Avincsal MO, Jimbo N, Fujikura K, Shinomiya H, Otsuki N, Morimoto K, et al. Epigenetic down-regulation of SOX2 is an independent poor prognostic factor for hypopharyngeal cancers. Histopathology 2017. https://doi.org/10.1111/his.13436.
[23] Chung JH, Jung HR, Jung AR, Lee YC, Kong M, Lee J-S, et al. SOX2 activation predicts prognosis in patients with head and neck squamous cell carcinoma. Sci Rep 2018:1–11. https://doi.org/10.1038/s41598-018-20086-w.
[24] Keysar SB, Astling DP, Anderson RT, Vogler BW, Bowles DW, Morton JJ, et al. A patient tumor transplant model of squamous cell cancer identifies PI3K inhibitors as candidate therapeutics in defined molecular bins. Mol Oncol 2013;7:776–90. https://doi.org/10.1016/j.molonc.2013.03.004.
[25] Schindelin J, Arganda-Carreras I, Frise E, Kaynig V, Longair M, Pietzsch T, et al. Fiji: an open-source platform for biological-image analysis. Nat Methods 2012;9:676–82. https://doi.org/10.1038/nmeth.2019.
[26] Gan GN, Eagles J, Keysar SB, Wang G, Glogowska MJ, Altunbas C, et al. Hedgehog signaling drives radioresistance and stroma-driven tumor repopulation in head and neck squamous cancers. Cancer Res 2014;74:7024–36. https://doi.org/10.1158/0008-5472.CAN-14-1346.
[27] Gan GN, Jimeno A. Emerging from their burrow: hedgehog pathway inhibitors for cancer. Expert Opin Investig Drugs 2016. https://doi.org/10.1080/13543784.2016.1216973.
[28] Pfister DG, Spencer S. NCCN clinical practice guidelines: head and neck cancers. Oral Dis 2017.
[29] Moore KA, Lemischka IR. Stem cells and their niches. Science 2006;311:1880–5. https://doi.org/10.1126/science.1110542.
[30] Sneddon JB, Werb Z. Location, location, Location: the cancer stem cell niche. Cell Stem Cell 2007;1:607–11. https://doi.org/10.1016/j.stem.2007.11.009.
[31] Oskarsson T, Batlle E, Massagué J. Metastatic stem cells: sources, niches, and vital pathways. Cell Stem Cell 2014;14:306–21. https://doi.org/10.1016/j.stem.2014.02.002.
[32] Plaks V, Kong N, Werb Z. The cancer stem cell niche: how essential is the niche in regulating stemness of tumor cells? Cell Stem Cell 2015;16:225–38. https://doi.org/10.1016/j.stem.2015.02.015.
[33] Kise K, Kinugasa-Katayama Y, Takakura N. Tumor microenvironment for cancer stem cells. Adv Drug Deliv Rev 2016;99:197–205. https://doi.org/10.1016/j.addr.2015.08.005.
[34] Prasetyanti PR, Medema JP. Intra-tumor heterogeneity from a cancer stem cell perspective. Mol Cancer 2017;16:41. https://doi.org/10.1186/s12943-017-0600-4.
[35] Jou A, Hess J. Epidemiology and molecular biology of head and neck cancer. Oncol Res Treat 2017;40:328–32. https://doi.org/10.1159/000477127.
[36] Leemans CR, Braakhuis BJM, Brakenhoff RH. The molecular biology of head and neck cancer. Nat Rev Cancer 2010;11:9–22. https://doi.org/10.1038/nrc2982.
[37] Shiozawa Y, Berry JE, Eber MR, Jung Y, Yumoto K, Cackowski FC, et al. The marrow niche controls the cancer stem cell phenotype of disseminated prostate cancer. Oncotarget 2016;7:41217–32. https://doi.org/10.18632/oncotarget.9251.
[38] Hermann PC, Bhaskar S, Cioffi M, Heeschen C. Cancer stem cells in solid tumors. Semin Cancer Biol 2010;20:77–84. https://doi.org/10.1016/j.semcancer.2010.03.004.